AIAA JOURNAL
Vol. 32, No. 6, June 1994

Fast Multigrid Method for Solving Incompressible Hydrodynamic Problems with Free Surfaces

J. Farmer,* L. Martinelli,† and A. Jameson‡
Princeton University, Princeton, New Jersey 08544

The focus of this work is the development of a finite-volume multigrid Euler scheme for solving three-dimensional, fully nonlinear ship wave problems. The flowfield and the a priori unknown free surface location are calculated by coupling the free surface kinematic and dynamic equations with the equations of motion for the bulk flow. The evolution of the free surface boundary condition is linked to the evolution of the bulk flow via a novel iteration strategy that allows temporary leakage through the surface before the solution is converged. The method of artificial compressibility is used to enforce the incompressibility constraint for the bulk flow. A multigrid algorithm is used to accelerate convergence to a steady state. The scheme is validated by comparing the numerical results with experimental results for the Wigley parabolic hull. Waterline profiles from bow to stern are in excellent agreement with the experimental results. The computed wave drag compares favorably with both theory and experiment for a wide range of Froude numbers. Overall, the present method proves to be accurate and efficient.

I. Introduction

THE modeling of aircraft flying in the transonic Mach number range has been the focus of great interest over the last two decades. This regime typically results in the most favorable cruise performance, but also produces flowfields with embedded regions of supersonic flow. The need to predict these complex flowfields has led to much progress in the numerical solution of compressible air flows about arbitrary bodies in recent years.[1] Unfortunately, the most successful methods for compressible flow simulation are not generally applicable to flows with low Mach numbers, and in the limit of truly incompressible flow, or zero Mach number, alternate methods must be used to compute the flowfield. As many of these methods have drawbacks, the purpose of the present work is to present a method for treating truly incompressible flows that retains the favorable characteristics of the recently developed compressible flow methods. The method is used here to predict waves on the free surface around a ship. In general, this problem retains many of the complexities associated with aircraft modeling, such as the need to predict the fluid flow characteristics about arbitrary fuselage/wing combinations (or hull/keel combinations for the hydrodynamic case). The ship wave problem is further complicated by the need to solve for the a priori unknown free surface location.

The fundamental problem in the prediction of incompressible flows, even flows without the complication of a free surface, is the loss of an evolution equation for the density. Because the density is constant, a time-independent constraint must be imposed on the momentum equations to ensure a divergence-free velocity field. In addition, the eigenvalues resulting from the system of conventional hyperbolic Euler equations for compressible flows become infinite in the limit of incompressible flow. This is due to the fact that incompressible flows exhibit infinite sound speeds. Thus, the well-established methods for computing compressible flows may not be used for the incompressible case.

Presented as Paper 93-0767 at the AIAA 31st Aerospace Sciences Meeting, Reno, NV, Jan. 11–14, 1993; received March 13, 1993; revision received Aug. 4, 1993; accepted for publication Sept. 18, 1993. Copyright © 1993 by the American Institute of Aeronautics and Astronautics, Inc. All rights reserved.

*Research Associate, Department of Mechanical and Aerospace Engineering. Member AIAA.

†Research Staff Member, Department of Mechanical and Aerospace Engineering. Member AIAA.

‡Professor, Department of Mechanical and Aerospace Engineering. Fellow AIAA.

The method of Hino[2] is a widely used approach for solving incompressible flow problems (see also the recent works of Miyata et al.[3] and Tahara et al.[4]).This method takes the divergence of the momentum equations and solves implicit equations at each time step for the pressure and the velocity fields such that continuity is satisfied. The method is expensive both because of the need to solve the implicit equations by an iterative method and because of the cost of calculating the divergence of the momentum equations in a curvilinear coordinate system.

The present work adopts the artificial compressibility method, an approach first proposed by Chorin[5] in 1967 as a method to solve viscous flows. Since then, Rizzi and Eriksson[6] have applied it to rotational inviscid flow, Dreyer[7] has applied it to low-speed, two-dimensional airfoils and Kodama[8] has applied it to ship hull forms with a rigid free surface. In addition, Turkel[9] has investigated more sophisticated preconditioners than those originally proposed by Chorin. The basic idea behind artificial compressibility is to introduce a pseudotemporal equation for the pressure through the continuity equation. This approach removes the difficulties associated with compressible flow formulations as the Mach number approaches zero. The eigenvalues of the original system are replaced with an artificial set that renders the new equations well-conditioned for numerical computation. When combined with multigrid acceleration procedures,[10–12] artificial compressibility proves to be particularly effective. Converged solutions of incompressible flows over three-dimensional, isolated wings are obtained in 25–50 cycles.

The general objective of this work is the development of a more efficient method to predict free surface wave phenomena. A multigrid Euler scheme using artificial compressibility is coupled with a free surface formulation in a new method[13] and comparisons made with available experimental data.[14] The method is efficient and allows for a straight forward extension to include viscous terms associated with Navier-Stokes equations and a turbulence model. With this extension it will be possible to predict both the free surface wave patterns and the frictional and induced drag components. Additional work will focus on hull/keel junctures inclined at realistic attack angles.

II. Mathematical Model

Figure 1 shows the reference frame and ship location as used in this work. A right-handed coordinate system $Oxyz$, with the origin fixed at midship on the mean free surface is established. The z direction is positive upwards, y is positive towards the starboard side, and x is positive in the aft direction. The freestream velocity

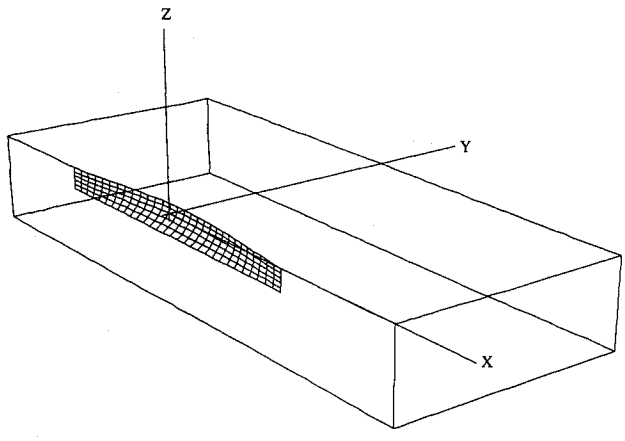

Fig. 1 Reference frame and ship location.

vector is parallel to the x axis and points in the same direction. The ship hull pierces the uniform flow and is held fixed in place, i.e., the ship is not allowed to sink (translate in z direction) or trim [rotate in (x, z) plane].

For a nonviscous incompressible fluid moving under the influence of gravity, the continuity and Euler equations may be put in the form,[2]

$$\begin{aligned} u_x + v_y + w_z &= 0 \\ u_t + uu_x + vu_y + wu_z &= -\psi_x \\ v_t + uv_x + vv_y + wv_z &= -\psi_y \\ w_t + uw_x + vw_y + ww_z &= -\psi_z \end{aligned} \tag{1}$$

Here $u = u(x, y, z, t)$, $v = v(x, y, z, t)$, and $w = w(x, y, z, t)$ are total velocity components in the x, y, z directions. All lengths and velocities are nondimensionalized by the ship length L and freestream velocity U, respectively. The pressure ψ is the static pressure p minus the hydrostatic component $-zFr^{-2}$ and may be expressed as $\psi = p + zFr^{-2}$, where $Fr = U/\sqrt{gL}$ is the Froude number. The pressure variable ψ is nondimensionalized by ρU^2. This set of equations will be solved subject to the following boundary conditions.

When the effects of surface tension and viscosity are neglected, the boundary condition on the free surface consists of two equations. The first, the dynamic condition, states that the pressure acting on the free surface is constant. The second, the kinematic condition, states that the free surface is a material surface: once a fluid particle is on the free surface, it forever remains on the surface. The dynamic and kinematic boundary conditions may be expressed as

$$p = \text{constant}, \qquad \frac{d\beta}{dt} = w = \beta_t + u\beta_x + v\beta_y \tag{2}$$

where $z = \beta(x, y, t)$ is the free surface location. Equation (2) only permits solutions where β is single valued. Consequently, it does not allow for the breaking of bow waves, which can often be observed with cruiser-type hulls. Breaking waves are difficult to treat numerically and are not considered in this work.

The remaining boundaries consist of the ship hull, the boundaries which comprise the symmetry portions of the meridian plane, and the far field of the computational domain. On the ship hull, the condition is that of impermeability and is stated simply by

$$\boldsymbol{q} \cdot \boldsymbol{n} = un_x + vn_y + wn_z = 0$$

where the normal vector $\boldsymbol{n}$ may be assumed to point into the flow. On the symmetry plane [that portion of the (x, z) plane excluding the ship hull], derivatives in the y direction as well as the v component of velocity are set to zero. The upstream plane has $u = U$ and $\psi = 0$ ($p = -zFr^{-2}$) with the v and w velocity components also set to zero. Similar conditions hold on the bottom plane which is assumed to represent infinitely deep water where no disturbances are felt. One-sided differences are used to update the flow variables on the starboard plane. A radiation condition should be imposed on the outflow domain to allow the wave disturbance to pass out of the computational domain. Although fairly sophisticated formulations may be devised to represent the radiation condition,[15] simple extrapolations proved to be sufficient in this work.

III. Numerical Solution

The formulation of the numerical solution procedure is based on a finite-volume method (FVM) for the bulk flow variables (u, v, w, and ψ), coupled to a finite-difference method for the free surface evolution variables (β and ψ). Alternative cell-centered and cell-vertex formulations may be used in finite-volume schemes.[10] A cell-vertex formulation is preferred in this work because values of the flow variables are needed on the boundary to implement the free surface boundary condition. The bulk flow is solved subject to Dirichlet conditions for the free surface pressure, followed by a free surface update via the bulk flow solution [i.e., constant values for the velocities in Eq. (2)]. Each formulation is explicit and uses local time stepping. Both multigrid and residual averaging techniques are used in the bulk flow to accelerate convergence.

A. Bulk Flow Solution

Following Chorin[5] and more recently Dreyer,[7] the governing set of incompressible flow equations may be written in vector form as

$$\frac{\partial \boldsymbol{w}}{\partial t^*} + \boldsymbol{P}\left(\frac{\partial \boldsymbol{f}}{\partial x} + \frac{\partial \boldsymbol{g}}{\partial y} + \frac{\partial \boldsymbol{h}}{\partial z}\right) = 0 \tag{3}$$

where the vector of dependent variables $\boldsymbol{w}$ and flux vectors $\boldsymbol{f}$, $\boldsymbol{g}$, and $\boldsymbol{h}$ are given by

$$\boldsymbol{w} = [\psi, u, v, w]^T$$

$$\boldsymbol{f} = [u, u^2 + \psi, uv, uw]^T$$

$$\boldsymbol{g} = [v, vu, v^2 + \psi, vw]^T$$

$$\boldsymbol{h} = [w, wu, wv, w^2 + \psi]^T$$

The preconditioning matrix $\boldsymbol{P}$ is given by

$$\boldsymbol{P} = \begin{bmatrix} \Gamma^2 & 0 & 0 & 0 \\ 0 & 1 & 0 & 0 \\ 0 & 0 & 1 & 0 \\ 0 & 0 & 0 & 1 \end{bmatrix}$$

where Γ^2 is called the artificial compressibility parameter due to the analogy that may be drawn between the preceding equations and the equations of motion for a compressible fluid whose equation of state is given by

$$p = \Gamma^2 \rho$$

Thus, ρ is an artificial density, and Γ may be referred to as an artificial sound speed. When the temporal derivatives tend to zero, the set of equations satisfy precisely the incompressible Euler equations, with the consequence that the correct pressure may be established using the artificial compressibility formulation. The preconditioning matrix $\boldsymbol{P}$ may be viewed as a device to create a well-posed system of hyperbolic equations that are to be integrated to steady state along lines similar to the well-established compressible flow FVM formulation.[12] In addition, the artificial compressibility parameter may be viewed as a relaxation parameter for the pressure iteration. Note also that temporal derivatives are now

denoted by t^* to indicate pseudotime; the artificial compressibility, as formulated in the present work, destroys time accuracy.

To demonstrate the effect of the preconditioning matrix on the preceding set of equations and to establish the hyperbolicity of the set, Eq. (3) may be written in quasilinear form to determine the eigenvalues.[6] The eigenvalues are found to be

$$\lambda_1 = U, \qquad \lambda_2 = U, \qquad \lambda_3 = U + a, \qquad \lambda_4 = U - a$$

where

$$U = u\omega_x + v\omega_y + w\omega_z$$

and

$$a^2 = U^2 + \Gamma^2(\omega_x^2 + \omega_y^2 + \omega_z^2)$$

The wave number components ω_x, ω_y, and ω_z are defined on $-\infty \le \omega_x, \omega_y, \omega_z \le +\infty$. Since the eigenvalues are real for any value of ω_x, ω_y, and ω_z, the system is hyperbolic.

The choice of Γ is crucial in determining the convergence and stability properties of the numerical scheme. Typically, the convergence rate of the scheme is dictated by the slowest system waves and the stability of the scheme by the fastest. In the limit of large Γ, the difference in wave speeds can be large. Although this situation would presumably lead to a more accurate solution through the penalty effect in the pressure equation, very small time steps would be required to ensure stability. Conversely, for small Γ, the difference in the maximum and minimum wave speeds may be significantly reduced, but at the expense of accuracy. Thus a compromise between the extremes is required. Following the work of Dreyer, the choice for Γ is taken to be

$$\Gamma^2 = C(u^2 + v^2 + w^2)$$

where C is a constant of order unity. In regions of high velocity and low pressure where suction occurs, Γ is large to improve accuracy, and in regions of lower velocity, Γ is correspondingly reduced.

The choice of Γ also influences the outflow boundary condition, or radiation condition. If it can be demonstrated that all system eigenvalues are both real and positive, then downstream or outflow boundary points may be extrapolated from the interior upstream flow. Even though an examination of the eigenvalues reveals that this can never be the case, the condition can be approached by a judicious choice of Γ. If Γ is large, extrapolation fails because the flow has both downstream and upstream dependence. As Γ is reduced, the upstream dependence becomes more pronounced and the downstream dependence is reduced. Eventually the upstream dependence is sufficiently dominant to allow extrapolation. Hence, all outflow variables are updated using zero gradient extrapolation.

Following the general procedures for FVM, the governing equations may be integrated over an arbitrary volume Ω. Application of the divergence theorem on the flux term integral yields

$$\frac{\partial}{\partial t^*}\int_\Omega \boldsymbol{w}\, d\Omega + \boldsymbol{P}\int_{\partial\Omega} (\boldsymbol{f}\, dS_x + \boldsymbol{g}\, dS_y + \boldsymbol{h}\, dS_z) = 0$$

where S_x, S_y, and S_z are the directed areas in the x, y, and z directions, respectively. The computational domain is divided into hexahedral cells. Application of FVM to each of the computational cells results in the following system of ordinary differential equations,

$$\frac{d}{dt^*}(V_{ijk}\boldsymbol{w}) + Q_{ijk} = 0$$

Here, the volume V_{ijk} is given by the summation of the eight cells surrounding node i, j, k and $Q_{ijk}(\boldsymbol{w})$ is defined as

$$Q_{ijk}(\boldsymbol{w}) = \sum_{k=1}^{n} (\boldsymbol{f}S_x + \boldsymbol{g}S_y + \boldsymbol{h}S_z)_k$$

where the summation is over the n faces surrounding V_{ijk}.

In practice, the grid is body fitted and hence non-Cartesian. A curvilinear transformation from the physical coordinate system to the computational coordinate system defined by

$$\xi = \xi(x, y, z), \qquad \eta = \eta(x, y, z), \qquad \zeta = \zeta(x, y, z)$$

is incorporated leading to a modified approach to the flux evaluation in the transformed space. The new approach becomes

$$Q_{ijk} = \frac{\partial \tilde{\boldsymbol{f}}}{\partial \xi} + \frac{\partial \tilde{\boldsymbol{g}}}{\partial \eta} + \frac{\partial \tilde{\boldsymbol{h}}}{\partial \zeta}$$

where

$$\tilde{\boldsymbol{f}} = J\{\tilde{u}, u\tilde{u} + \xi_x\psi, v\tilde{u} + \xi_y\psi, w\tilde{u} + \xi_z\psi\}^T$$

$$\tilde{\boldsymbol{g}} = J\{\tilde{v}, u\tilde{v} + \eta_x\psi, v\tilde{v} + \eta_y\psi, w\tilde{v} + \eta_z\psi\}^T$$

$$\tilde{\boldsymbol{h}} = J\{\tilde{w}, u\tilde{w} + \zeta_x\psi, v\tilde{w} + \zeta_y\psi, w\tilde{w} + \zeta_z\psi\}^T$$

and $\Delta\xi = \Delta\eta = \Delta\zeta = 1$. The contravariant velocity components $\tilde{u}$, $\tilde{v}$, and $\tilde{w}$ are given by

$$\tilde{u} = u\xi_x + v\xi_y + w\xi_z$$

$$\tilde{v} = u\eta_x + v\eta_y + w\eta_z$$

$$\tilde{w} = u\zeta_x + v\zeta_y + w\zeta_z$$

The Jacobian of the transformation is denoted by J and ξ_x, η_x ... are identified with the grid metrics. In practice, the terms $J\xi_x$, $J\eta_x$ ... , required in the flux terms, are identified with the projected areas of each cell face. They are computed by taking the cross product of the two vectors joining opposite corners of each cell face in the body-fitted coordinate system. The physical variables required in the transformed flux evaluation may be averaged on each cell face through the four nodal values associated with each face.

This scheme reduces to a second-order accurate, nondissipative central difference approximation to the Euler equations on sufficiently smooth grids. A central difference scheme permits odd-even decoupling at adjacent nodes which may lead to oscillatory solutions. To prevent this unphysical phenomena from occurring, a dissipation term is added to the system of equations such that the system now becomes

$$\frac{d}{dt^*}(V_{ijk}\boldsymbol{w}) + \boldsymbol{P}[Q_{ijk}(\boldsymbol{w}) - D_{ijk}(\boldsymbol{w})] = 0 \tag{4}$$

For the present problem a third-order background dissipation term is added. The dissipative term is constructed in such a manner that the conservation form of the system of equations is preserved. The dissipation has the form

$$D_{ijk}(\boldsymbol{w}) = D_\xi + D_\eta + D_\zeta \tag{5}$$

where

$$D_{\xi ijk} = d_{\xi i+1,j,k} - d_{\xi i,j,k}$$

and

$$d_{\xi i,j,k} = \alpha\delta_\xi^2(\boldsymbol{w}_{i+1,j,k} - \boldsymbol{w}_{i,j,k}) \tag{6}$$

Similar expressions may be written for the η and ζ directions with δ_ξ^2, δ_η^2, δ_ζ^2 representing second difference central operators.

In Eq. (6), the dissipation coefficient α is a scaling factor, proportional to the local wave speed. The actual form for the coeffi-

cient is based on the spectral radius of the system and is given in the ξ direction as

$$\alpha = \varepsilon[J|\tilde{u}| + \Gamma(S_x^2 + S_y^2 + S_z^2)^{1/2}]$$

where $\tilde{u}$ is the contravariant velocity component and S_x, S_y, and S_z are the directed face areas. Similar dissipation coefficients are used for the η and ζ components in Eq. (5). The ε term is used to manually adjust the amount of dissipation.

Equation (4) is integrated in time by an explicit multistage scheme. For each bulk flow time step, the grid, and thus V_{ijk}, is independent of time. Hence Eq. (4) can be written as

$$\frac{dw_{ijk}}{dt^*} + R_{ijk}(w) = 0 \tag{7}$$

where

$$R_{ijk}(w) = \frac{1}{V_{ijk}} P(Q_{ijk} - D_{ijk})$$

The actual time step Δt is limited by the Courant number (CFL), which states that the fastest waves in the system may not be allowed to propagate farther than the smallest grid spacing over the course of a time step. In this work, local time stepping is used such that regions of large grid spacing are permitted to have relatively larger time steps than regions of small grid spacing. Of course the system wave speeds vary locally and must be taken into account as well. The final local time step is thus computed as

$$\Delta t^*_{ijk} = \frac{(\mathrm{CFL})\, V_{ijk}}{\lambda_{ijk}}$$

where λ_{ijk} is the sum of the spectral radii in the x, y, and z directions. In regions of small grid spacing and/or regions of high characteristic wave velocities, the time step will be smaller than elsewhere.

The allowable Courant number may be increased by smoothing the residuals at each stage using the following product form in three dimensions

$$(1 - \varepsilon_\xi \delta_\xi^2)(1 - \varepsilon_\eta \delta_\eta^2)(1 - \varepsilon_\zeta \delta_\zeta^2)\bar{R} = R$$

where ε_ξ, ε_η, and ε_ζ are smoothing coefficients and the $\delta^2_{\xi,\eta,\zeta}$ are central difference operators in computational coordinates. Each residual R_{ijk} is thus replaced by an average of itself and the neighboring residuals.

Very rapid convergence to a steady state is achieved with the aid of a multigrid procedure. The idea behind the multigrid strategy is

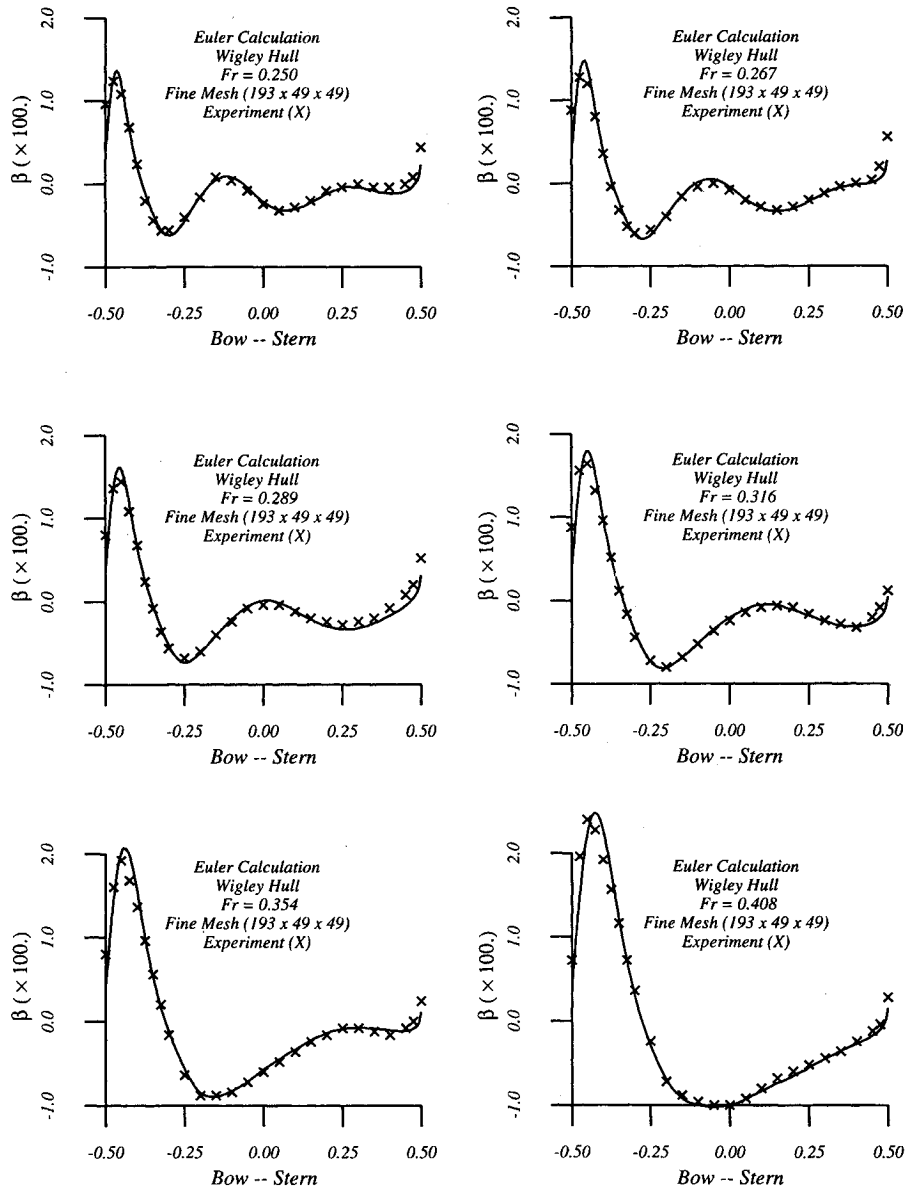

Fig. 2 Wigley parabolic hull wave profiles.

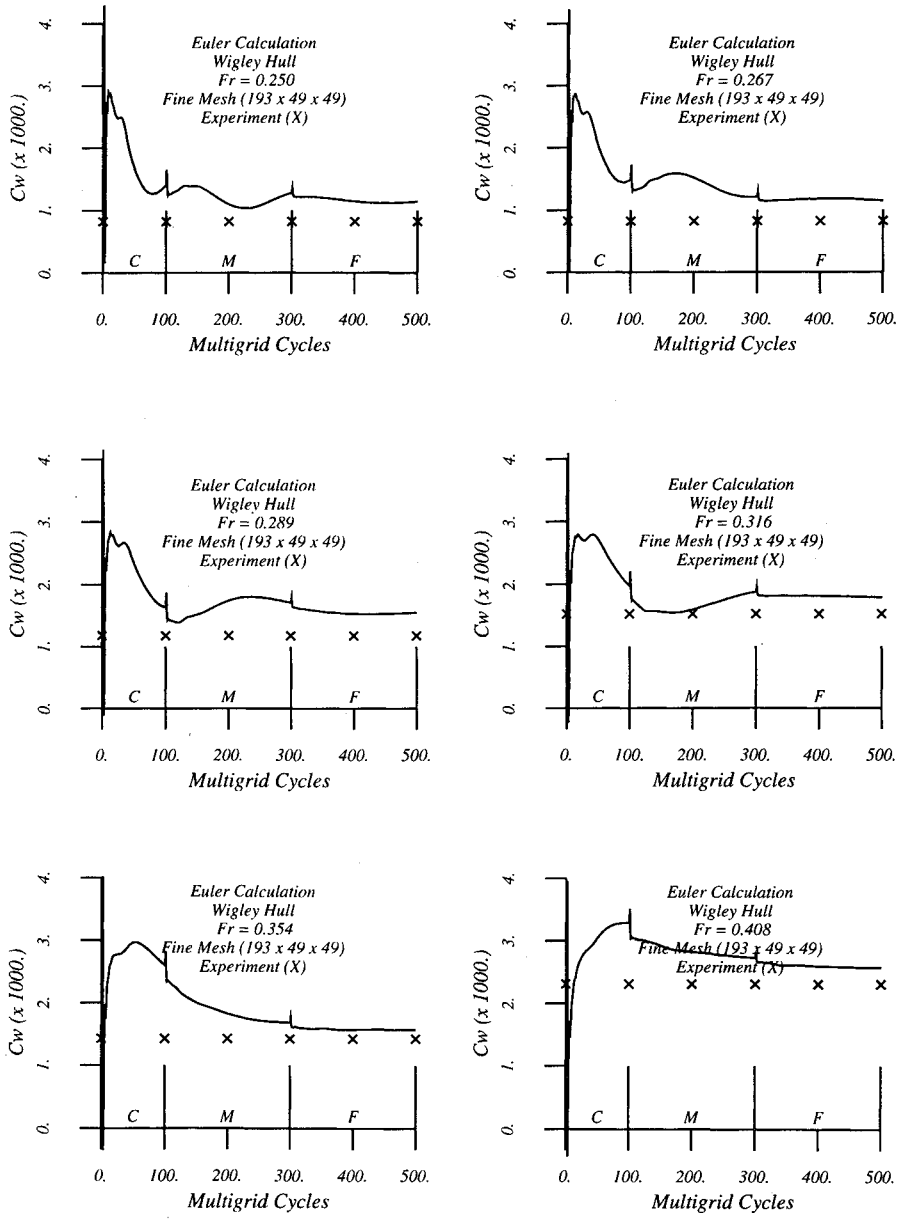

Fig. 3 Wigley parabolic hull wave resistance history.

to accelerate the evolution of the system of equations on the fine grid by introducing auxiliary calculations on a series of coarser grids. The coarser grid calculations introduce larger scales and larger time steps with the result that low-frequency error components may be efficiently and rapidly damped out. Auxiliary grids are introduced by doubling the grid spacing, and values of the flow variables are transferred to a coarser grid by the rule

$$w_{2h}^{(0)} = T_{2h,h} w_h$$

where the subscripts denote values of the grid spacing parameter (i.e., h is the finest grid, $2h$, $4h$, ... are successively coarser grids) and $T_{2h,h}$ is a transfer operator from a fine grid to a coarse grid. The transfer operator picks flow variable data at alternate points to define coarser grid data as well as the coarser grid itself. A forcing term is then defined as

$$P_{2h} = \sum R_h(w_h) - R_{2h}(w_{2h}^{(0)})$$

where R is the residual of the difference scheme. To update the solution on the coarse grid, the multistage scheme is reformulated as

$$w_{2h}^{(1)} = w_{2h}^{(0)} - \alpha_1 \Delta t^* (R_{2h}^{(0)} + P_{2h})$$

...

$$w_{2h}^{(q+1)} = w_{2h}^{(0)} - \alpha_q \Delta t^* (R_{2h}^{(q)} + P_{2h})$$

...

where $R^{(q)}$ is the residual of the qth stage. In the first stage, the addition of P_{2h} cancels $R_{2h}(w^{(0)})$ and replaces it by $\Sigma R_h(w_h)$, with the result that the evolution on the coarse grid is driven by the residual on the fine grid. The result $w_{2h}^{(m)}$ now provides the initial data for the next grid $w_{4h}^{(0)}$ and so on. Once the last grid has been reached, the accumulated correction must be passed back through successively finer grids. Assuming a three-grid scheme, let $w_{4h}^{(+)}$ represent the final value of w_{4h}. Then the correction for the next-finer grid will be

$$w_{2h}^{(+)} = w_{2h}^{(m)} + I_{2h,4h}(w_{4h}^{(+)} - w_{4h}^{(0)})$$

where $I_{a,b}$ is an interpolation operator from the coarse grid to the next finer grid. The final result on the fine grid is obtained in the same manner:

$$w_h^{(+)} = w_h^{(m)} + I_{h,2h}(w_{2h}^{(+)} - w_{2h}^{(0)})$$

The process may be performed on any number of successively coarser grids. The only restriction in the present work being use of

a structured grid whereby elements of the coarsest grid do not overlap the ship hull. A three-level "*W*-cycle" is used in the present work for each time step on the fine grid.[12]

The multigrid acceleration procedure is embedded in a grid refinement procedure to further reduce the computer time required to achieve steady-state solutions on finely resolved grids. In the grid refinement procedure the flow equations are solved on coarse grids in the early stages of the simulation. The coarse grids permit large time steps, and the flowfield and the wave pattern evolve quite rapidly. When the wave pattern approaches a steady state, the grid is refined by doubling the number of grid points in all directions and the flow variables and free surface location are interpolated onto the new grid. Computations then continue using the finer grid with smaller time steps. The multigrid procedure is applied at all stages of the grid refinement to accelerate the calculations on each grid in the sequence, producing a composite "full multigrid" scheme which is extremely efficient.

B. Free Surface Solution

Both a kinematic and dynamic boundary condition must be imposed at the free surface. For the fully nonlinear condition, the free surface must move with the flow (i.e., up and down corresponding to the wave height and location) and the boundary conditions are applied on the distorted free surface. Equation (2) can be cast in a form more amenable to numerical computations by introducing a curvilinear coordinate system that transforms the curved free surface $\beta(x, y)$ into computational coordinates $\beta(\xi, \eta)$. This results in the following transformed kinematic condition

$$\beta_{t^*} + U\beta_\xi + V\beta_\eta = w \tag{8}$$

where U and V are contravariant velocity components given by

$$U = u\xi_x + v\xi_y$$

$$V = u\eta_x + v\eta_y$$

The free surface kinematic equation may now be expressed as

$$\frac{d\beta_{ij}}{dt^*} + Q_{ij}(\beta) = 0$$

where $Q_{ij}(\beta)$ consists of the collection of velocity and spacial gradient terms which result from the discretization of Eq. (8). Note that this is not the result of a volume integration and thus the volume (or actually area) term does not appear in the residual as in the FVM formulation. Throughout the interior of the (x, y) plane, all derivatives are computed using the second-order centered difference stencil in computational coordinates ξ and η. On the boundary, a second-order centered stencil is used along the boundary tangent and a first-order, one-sided difference stencil is used in the boundary normal direction.

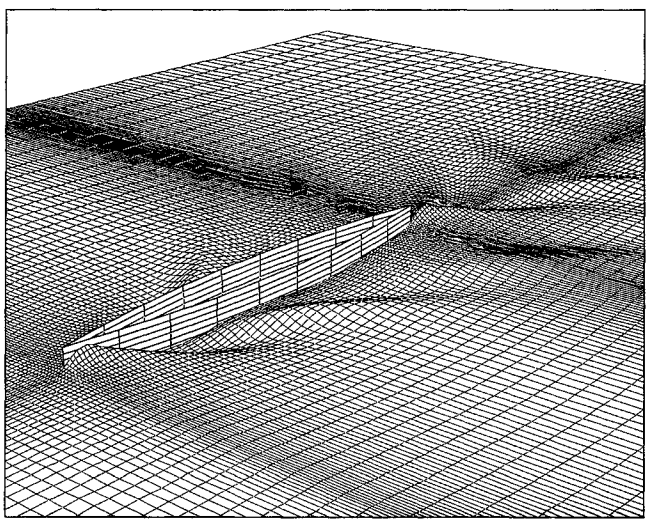

Fig. 4 Perspective view of wave elevation, $Fr = 0.2670$ (wave elevation multiplied three times).

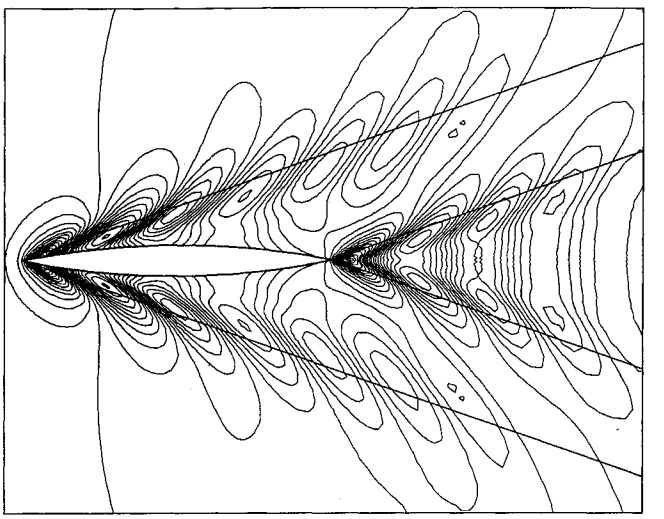

Fig. 5 Overhead view of wave elevation (or pressure ψ) contours, $Fr = 0.2670$.

As was necessary in the FVM formulation for the bulk flow, background dissipation must be added to prevent decoupling of the solution. The method used to compute the dissipation terms borrows from a two-dimensional FVM formulation and appears as follows:

$$D_{ij} = D_\xi + D_\eta$$

where

$$D_{\xi ij} = d_{\xi i+1,j} - d_{\xi i,j}$$

and

$$d_{\xi i,j} = \alpha\delta_\xi^2(\beta_{i+1,j} - \beta_{i,j})$$

The expression for α may be written as

$$\alpha = \varepsilon(|U_{i+1,j}| + |U_{i,j}|)$$

where $U_{i,j}$ is the unscaled contravariant velocity component defined by

$$U = uy_\eta - vx_\eta$$

Hence the system of equations for the free surface is expressed as

$$\frac{d\beta_{ij}}{dt^*} + R_{ij}(\beta) = 0$$

where

$$R_{ij} = Q_{ij} - D_{ij}$$

The time-stepping scheme defined by Eq. (7) is also used here. Once the free surface update is accomplished, the pressure is adjusted on the free surface such that

$$\psi^{(n+1)} = \beta^{(n+1)}Fr^{-2}$$

The free surface and the bulk flow solutions are coupled by first computing the bulk flow at each time step, and then using the bulk flow free surface velocities to calculate the movement of the free surface. After the free surface elevation is updated, its new values are used as a boundary condition for the pressure on the bulk flow for the next time step. The entire iterative process, in which both

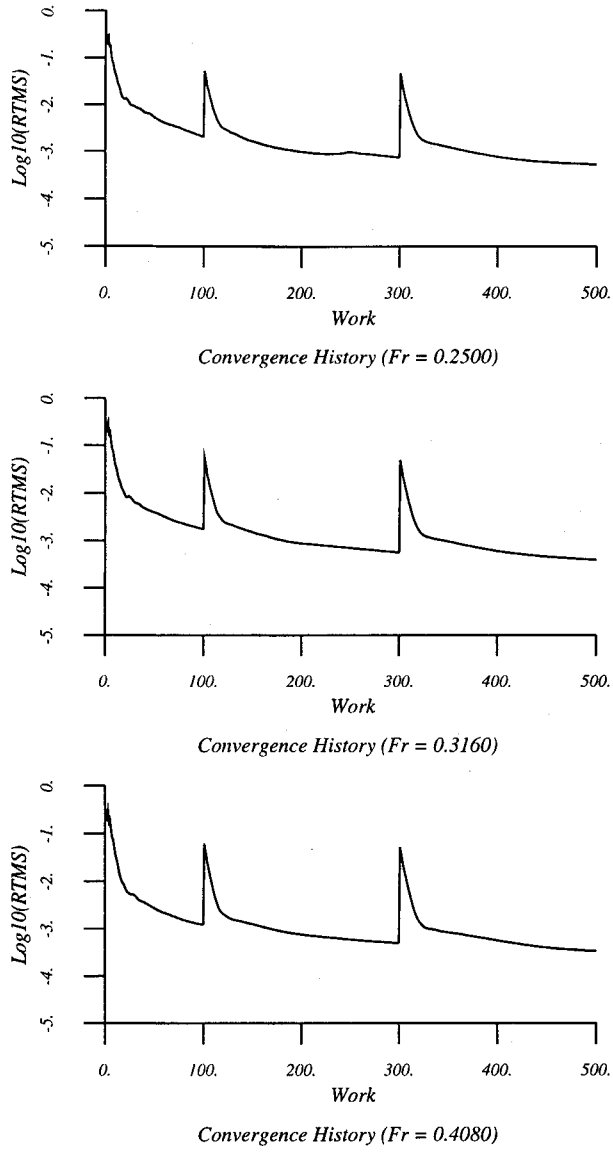

Fig. 6 Convergence history.

the bulk flow and the free surface are updated at each time step, is repeated until some measure of convergence is attained; usually a steady-state wave profile and wave resistance coefficient.

Since the free surface is a material surface, the flow must be tangent to it in the final steady state. During the iterations, however, the flow is allowed to leak through the surface as the solution evolves towards the steady state. This leakage, in effect, drives the evolution equation. Suppose that at some stage, the vertical velocity component w is positive [cf. Eq. (2) or (8)]. Provided that the other terms are small, this will force β^{n+1} to be greater than β^n. When the time step is complete, ψ is adjusted such that $\psi^{n+1} > \psi^n$. Because the free surface has moved farther away from the original undisturbed upstream elevation and the pressure correspondingly increased, the velocity component w [or better still $\boldsymbol{q} \cdot \boldsymbol{n}$ where $\boldsymbol{n} = \nabla F/|\nabla F|$ and $F = z - \beta(x, y)$] will then be reduced. This results in a smaller $\Delta\beta$ for the next time step. The same is true for a negative vertical velocity, in which case there is mass leakage into the system rather than out. Only when steady state has been reached is the mass flux through the surface zero and tangency enforced. In fact, the residual flux leakage could be used in addition to drag components and pressure residuals as a measure of convergence to the steady state.

IV. Results for the Wigley Parabolic Hull

To validate the method we have performed calculations on the well-known Wigley parabolic hull, for which extensive experimental data is available. Figure 2 shows the computed wave profiles, from bow to stern along the hull, compared with experiments conducted at the University of Tokyo.[14] The agreement with experiment is extremely good. Wavelength, and the amplitudes at all peaks and troughs, are in excellent agreement with experiment. The only discrepancy noted is near the stern where separation and eddy losses, albeit small, may be present in the experiments.

Figure 3 shows the computed wave drag vs the experimentally determined wave drag as the simulation proceeds. The computed wave drag is found by integrating the longitudinal component of the static pressure over the wetted surface of the hull. The experimental wave drag is inferred by subtracting an estimate of the friction drag from the total drag or by wave analysis. Note that the computed wave drag is evaluated after each multigrid cycle and hence the evolution of the drag is plotted vs the experimentally determined steady-state wave drag (marked by the x's). The capital letters C, M, and F refer to coarse, medium, and fine grids, respectively, in the grid refinement procedure. For each Froude number, the computed wave drag overpredicts the experimentally determined wave drag by a small amount. This overprediction may arise from the comparison of viscous experiments with a purely inviscid numerical scheme. It remains to incorporate the viscous terms and make a more meaningful comparison of the wave drag via Navier-Stokes calculations. Aside from the overprediction, the computed steady-state wave drag follows the general trend predicted by the Michell theory; interference between bow and stern wakes lead to oscillations in a wave drag vs ship velocity curve.[16]

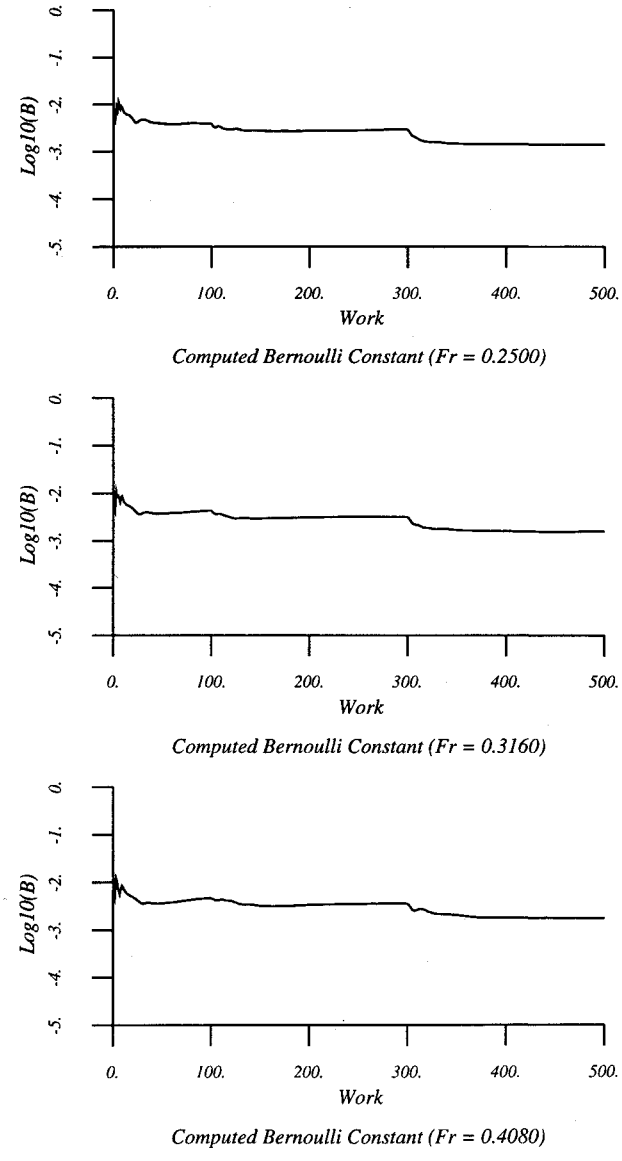

Fig. 7 Computed Bernoulli constant.

Figure 4 shows a perspective view of the final distorted grid for the case $Fr = 0.2670$ (the wave elevation has been magnified for clarity). Figure 5 shows an overhead view of the wave elevation contours β, or the free surface pressure contours $\psi = Fr^{-2}\beta$, for the same case. The divergent and transverse wave patterns, originating from both bow and stern, are in excellent agreement with the patterns predicted by the linear Kelvin theory[17]; the waves are confined by straight line sectors of ± 19.46 deg.

Figures 6 and 7 show convergence history of the pressure residual and computed free surface Bernoulli constant for various Froude numbers as the simulation proceeds. The pressure residual, computed by taking the root mean square of $d\psi/dt$, provides an important measure of the error in divergence of mass, as evident from the continuity equation of the vector system 3:

$$\frac{1}{\Gamma^2}\frac{\partial \psi}{\partial t^*} + \nabla \cdot \boldsymbol{q} = 0$$

As shown in Fig. 6, the computed residual is small implying that Eq. (1) is nearly satisfied. It is probably the "leap frog" nature of the iterative scheme that prevents the error from becoming smaller; the bulk flow solution and free surface solution continually adjust each other, leading to minute oscillations in free surface height and pressure ($\Delta\beta \approx 10^{-6}$). The Bernoulli constant B is computed by summing all the free surface nodal values of

$$B_{ij} = {}^1/_2(\boldsymbol{q} \cdot \boldsymbol{q} - 1)_{ij} + \psi_{ij}$$

and dividing by the number of free surface nodes. This quantity represents another measure of convergence of the scheme since it is fairly constant and close to the expected value of zero.

A final comment with regard to convergence and accuracy is that the information desired from the simulation, usually wave drag, can be obtained in approximately 100 multigrid cycles on the fine grid following the coarse- and medium-grid computations. One can see from Figs. 3, 6, and 7 that the wave drag, pressure residual, and Bernoulli constant change little beyond this point. What will change is the continuing evolution of the downstream wave profile, but this evolution has little effect on the computed drag once the profile near the ship hull has been established.

V. Conclusions

The objective of the present work was to develop an accurate and efficient method to compute incompressible Euler solutions for the nonlinear ship wave problem. The results for the Wigley hull validate the method for the range of test cases examined. The wave elevations predicted by the numerical simulations are in excellent agreement with the experimental measurements. The computed wave drag is in good agreement with the wave drag inferred from the experimental results.

The computational time for the simulations is approximately 10 h for the Euler calculations on the Wigley hull. These simulations consist of 100 steps on a $49 \times 13 \times 13$ grid, 200 steps on a $97 \times 25 \times 25$ grid, and 200 steps on a $193 \times 49 \times 49$ grid. The CPU time was recorded in calculations using a single-processor Convex 3400 computer with 64-bit arithmetic. For the given resolution the run times appear to represent about a tenfold decrease in the CPU times reported in the earlier literature, which have usually been presented for coarser grids. The CPU time required for the free surface update and regriding procedures was approximately 7% of that required for the bulk flow calculations.

We plan to extend the method to include viscous fluxes and a turbulence model. In addition to allowing the prediction of the friction drag, these improvements may also facilitate more accurate comparisons of the wave drag with experimental results. A status report may be found in Ref. 18. We also intend to simulate an actual sailing yacht with attached keel at a nonzero angle of attack.

Acknowledgments

Partial support for this work was provided through Office of Naval Research Grant N00014-89-J-1366 and Defense Advanced Research Projects Agency Grant N00014-89-J-0759. This support is gratefully acknowledged by the authors.

References

[1]Jameson, A., Baker, T., and Weatherill, N., "Calculation of Inviscid Transonic Flow Over a Complete Aircraft," AIAA Paper 86-0103, Jan. 1986.

[2]Hino, T., "Computation of Free Surface Flow Around an Advancing Ship by the Navier-Stokes Equations," *Proceedings, Fifth International Conference on Numerical Ship Hydrodynamics* (Hiroshima, Japan), National Academy Press, Washington, DC, 1989, pp. 103–117.

[3]Miyata, H., Toru, S., and Baba, N., "Difference Solution of a Viscous Flow with Free-Surface Wave about an Advancing Ship," *Journal of Computational Physics,* Vol. 72, 1987, pp. 393–421.

[4]Tahara, Y., Stern, F., and Rosen, B., "An Interactive Approach for Calculating Ship Boundary Layers and Wakes for Nonzero Froude Number," *Journal of Computational Physics,* Vol. 98, No. 1, 1992, pp. 33–53.

[5]Chorin, A., "A Numerical Method for Solving Incompressible Viscous Flow Problems," *Journal of Computational Physics,* Vol. 2, No. 1, 1967, pp. 12–26.

[6]Rizzi, A., and Eriksson, L., "Computation of Inviscid Incompressible Flow with Rotation," *Journal of Fluid Mechanics,* Vol. 153, April 1985, pp. 275–312.

[7]Dreyer, J., "Finite Volume Solutions to the Unsteady Incompressible Euler Equations on Unstructured Triangular Meshes," M.S. Thesis, Mechanical and Aerospace Engineering Dept., Princeton Univ., Princeton, NJ, June 1990.

[8]Kodama, Y., "Grid Generation and Flow Computation for Practical Ship Hull Forms and Propellers Using the Geometrical Method and the IAF Scheme," *Proceedings, Fifth International Conference on Numerical Ship Hydrodynamics* (Hiroshima, Japan), National Academy Press, Washington, DC, 1989, pp. 71–85.

[9]Turkel, E., "Preconditioned Methods for Solving the Incompressible and Low Speed Compressible Equations," Inst. for Computer Applications in Science and Engineering, Rept. 86-14, NASA Langley Research Center, Hampton, VA, March 1986.

[10]Jameson, A., "Solution of the Euler Equations for Two Dimensional Transonic Flow by a Multigrid Method," *Applied Mathematics and Computation,* Vol. 13, Nos. 3 and 4, 1983, pp. 327–356.

[11]Jameson, A., "Computational Transonics," *Communications on Pure and Applied Mathematics,* Vol. 41, No. 3, 1988, pp. 507–549.

[12]Jameson, A., "A Vertex Based Multigrid Algorithm For Three Dimensional Compressible Flow Calculations," *Numerical Methods for Compressible Flow—Finite Difference, Element and Volume Techniques,* edited by T. E. Tezduar and T. J. R. Hughes, American Society of Mechanical Engineers, Publication of AMD78, 1986.

[13]Farmer, J., "A Finite Volume Multigrid Solution to the Three Dimensional Nonlinear Ship Wave Problem," Ph.D. Thesis, Mechanical and Aerospace Engineering Dept., Princeton Univ., Princeton, NJ, Jan. 1993.

[14]Anon., "Cooperative Experiments on Wigley Parabolic Models in Japan," *17th ITTC Resistance Committee Report,* 2nd ed., Univ. of Tokyo, Tokyo, Japan, 1983, Chaps. 3 and 5.

[15]Orlanski, I., "A Simple Boundary Condition for Unbounded Hyperbolic Flows," *Journal of Computational Physics,* Vol. 21, No. 3, 1976, pp. 251–269.

[16]Wehausen, J. V., "The Wave Resistance of Ships," *Advances in Applied Mechanics,* Vol. 13, 1973, pp. 93–245.

[17]Stoker, J. J., *Water Waves,* Interscience, New York, 1957, Chap. 8.

[18]Farmer, J., Martinelli, L., and Jameson, A., "A Fast Multigrid Method for Solving the Nonlinear Ship Wave Problem with a Free Surface," *Proceedings, Sixth International Conference on Numerical Ship Hydrodynamics* (Iowa City, IA), Aug. 1993 (to be published).